Chem

CellPress

Thermally-gated bioorthogonal nanozymes with supramolecularly confined porphyrin catalysts for antimicrobial uses

Roberto Cao-Milán, Sanjana Gopalakrishnan, Luke D. He, Rui Huang, Li-Sheng Wang, Laura Castellanos, David C. Luther, Ryan F. Landis, Jessa Marie V. Makabenta, Cheng-Hsuan Li, Xianzhi Zhang, Federica Scaletti, Richard W. Vachet, and Vincent M. Rotello*

Department of Chemistry, University of Massachusetts Amherst, 710 North Pleasant Street, Amherst, Massachusetts 01003, USA.

*Lead Contact and Corresponding author: Vincent M. Rotello
Correspondence: rotello@chem.umass.edu
Phone: (+1) 413-545-2058
Fax: (+1) 413-545-4490

SUMMARY

Bioorthogonal catalysis has the capability of localized generation of imaging and therapeutic molecules *in vitro* and *in vivo*. The integration of these catalysts into thermoresponsive nanoparticle platforms would generate bioorthogonal 'nanozymes' that could be controlled through endogenous or exogenous thermal control. We have fabricated thermoresponsive nanozymes by confining supramolecular assemblies of porphyrins into the monolayer of gold nanoparticles. The resulting nanodevices feature an on-off gated thermal response occurring over a 3°C range with commensurate tunability of activation temperature from 25-37°C. Reversible activation of catalysis was demonstrated in complex biological environments, and the efficacy of bi-stable thermoresponsive nanozymes demonstrated through thermal activation of antibiotic-based prodrugs to effectively treat bacterial biofilms.

Thermoresponsive, nanocatalysts, antimicrobial activity, gold nanoparticles, iron porphyrins, nanozymes

INTRODUCTION

Bioorthogonal chemistry provides a tool for biological and biomedical science that uses abiotic chemical reactions that do not interfere with endogenous enzymatic processes. [1, 2] Bioorthogonal catalysis extends this capability to generate imaging and therapeutic agents on demand through enzyme-like activation of prodrugs and pro-fluorophores. [3, 4, 5]

The integration of bioorthogonal catalytic systems such as transition metal catalysts (TMCs) into nanoparticle hosts provides catalysts that replicate key features of enzymes.[6, 7, 8] The nanoparticle scaffolds of these nanozymes solubilize and stabilize catalysts in complex biological milieus.[9] Additionally, these scaffolds can be used to regulate the activity of the catalytic center, using supramolecular interactions to provide exogenous activation of catalysis in cells, as well as

providing complex kinetic behavior replicating enzymatic catalysis.[10, 11, 12]These bioinspired nanodevices with programable catalytic properties are especially appealing for biomedical applications where repetitive localized therapy is required such as biofilm infections.[13, 14] Spatiotemporally controlled generation of antibiotics could facilitate generation of therapeutic strategies with reduced side-effects.[15]

Thermally-responsive systems provide a means of controlling catalysis that would allow the regulation of bioorthogonal processes using endogenous or exogenous temperature gradients.[16] Most existing methods for creating thermoresponsive catalysts involve the insertion of either heterogeneous[17, 18, 19, 20] or molecular[21, 22] catalytic species into temperature-sensitive scaffolds such as polymers[7, 10, 17, 18, 19, 20] or gels[23, 24, 25, 26, 27, 28]. These systems modulate their catalytic activity through temperature-driven changes in volume and/or hydrophobicity of the scaffold, [29] thereby controlling the access of substrates to active sites[7, 18]. As a result, these systems generally exhibit attenuation in their catalytic properties with increasing temperature,[7, 17] providing turn-off based regulation that is challenging to translate to many biomedical applications.

In our previous studies we incorporated hydrophobic transition metal catalysts (TMCs) into the monolayer of 2 nm gold nanoparticles (NPs), [7, 30, 31, 32] to generate nanozymes that were functional in complex biological environments[30, 31, 32]. We hypothesized that beyond solubilizing and stabilizing the TMCs, we could use the confinement provided by the monolayer[33] to regulate intercatalyst supramolecular assemblies, providing a new approach to the thermoregulation of catalysis. (**Figure 1**, See also **SI-1,2 and 3**). For these studies we employed iron (III) tetraphenyl porphyrin (FeTPP), a system readily capable of self-assembly through stacking (**Figure 1a**).[34, 35] At low temperatures, the confined FeTPP assemblies display cooperative interactions with the ligands of the NP scaffold (**Figure 1c**), forming a compact structure that blocks substrate access to the active centers, thus deactivating the catalytic process.

An increase in temperature triggers the disassembly and redistribution of TMCs within the monolayer of NPs, enabling substrates to access the active centers and reactivating catalysis (**Figure 1d**). Activation occurred over a very narrow (3°C) range, providing bi-stable off-on control. Changing the FeTPP/NP stoichiometry enabled fine control of the gating temperature over the physiologically relevant range of 25-37 °C, with a resolution of 3°C. The inherent biostability of the AuNP platform yielded nanozymes that retain their thermal gating properties in complex biological environments. The potential of this platform for bioorthogonal therapy was demonstrated through a thermally regulated treatment of bacterial biofilms via the catalytic uncaging of antibiotic-based pro-drugs. On the whole, this platform presents a new tool for the gated thermal regulation of biosystems through bioorthogonal catalysis.

RESULTS AND DISCUSSION

Design and synthesis of a thermoresponsive nanozyme.

Nanozymes (NZs) were prepared by incorporating FeTPP into AuTTMA scaffolds. The FeTPP molecule catalyzes the reduction of aryl azides to the corresponding amines[36] providing a robust and efficient bioorthogonal catalyst that self-assembles into stacked aggregates (See **SI-9** for substrate design strategies). The host NPs

use the biocompatible scaffold used in our prior nanozyme systems that provides a hydrophobic environment for catalyst encapsulation.[7]

Nanozymes with different activation temperatures (**Figure 2**) were fabricated by mixing AuTTMA aqueous solutions (10 μM) with FeTPP solutions (THF) of concentrations ranging from 0.28 μM – 2.84 mM (See **SI-5**). Dynamic light scattering measurements showed no change in size of the AuNPs after encapsulation of the FeTPP assemblies (See **SI-1**), indicating retention of nanopartricle architecture and absence of aggregation. The incorporation of FeTPP assemblies of different sizes into NPs produced a family of thermoresponsive nanozymes **Fe-NZ_25**, **Fe-NZ_28**, **Fe-NZ_31**, **Fe-NZ_34** and **Fe-NZ_37** with different activation temperatures ranging from 25-37 °C (See **SI-2,5**).

The catalytic properties of the nanozymes were studied in PBS buffer through the activation of a non-fluorescent resorufin-based profluorophore (pro-Res, **Figure 1b**), where reduction of the azide results in fragmentation and release of the fluorescent resorufin molecule (**Figure 1 b**).

Demonstrating the reversibility and tunability of thermoresponsive behavior

Catalytic activity for each nanozyme was measured by monitoring changes in the fluorescence intensity of pro-Res solutions at different temperatures (Ex. 568 nm and Em. 588 nm). The FeTPP/AuTTMA stoichiometry was quantified using ICP-MS. Table 1 summarizes the ratio of FeTPP/AuTTMA in each nanozyme and their corresponding rates for activation of substrates at their respective temperatures of activation. **Figure 2a** shows turn-on of catalysis for each nanozyme at their respective temperatures of activation. Similar catalytic activity across different nanozymes was observed at their activation temperature (**Figure 2a and Table 1**) consistent with the nanozymes having a similar number of accessible FeTPP when they activate. In contrast, at 45 °C the catalytic efficiency of nanozymes is proportional to the amount of encapsulated FeTPP, indicating that at such temperatures most of encapsulated FeTPP are dissociated and catalytically active(See **SI-10**).

Fe-NZ	FeTPP/ NP (molecules/ particle)	V_{TA} (mol [NZ(mol)]$^{-1}$ min^{-1})
Fe-NZ_25	4 ± 1	98.17 ± 8.448
Fe-NZ_28	8 ± 1	100.2 ± 30.11
Fe-NZ_31	9 ± 1	86.74 ± 4.7008
Fe-NZ_34	14 ± 2	123.2 ± 20.90
Fe-NZ_37	28 ± 3	113.1 ± 14.19

Table 1 Number of FeTPP molecules encapsulated in each Fe-NZ and the rate of substrate activation of each nanozyme at its activation temperature. Catalytic activity was tracked by monitoring changes in fluorescence of pro-Res solutions (Ex. 568 nm, Em. 588 nm).

The mixture of FeTPP solutions in THF with water instantly produced assemblies of different sizes based on the concentration of FeTPP solution, as inferred from UV-Vis analyses. These FeTPP assemblies are confined in the AuTTMA scaffold to obtain nanozymes. It is expected that FeTPP assemblies of smaller sizes would have lower contact with the ligands of the AuTTMA scaffold, thereby reducing the

strength of hydrophobic interactions. As a result, the assemblies are expected to disaggregate into their open conformations at lower temperatures, thereby providing access of active centers to the substrates. Conversely, FeTPP assemblies of larger sizes would require higher temperatures to generate their open conformations, due to stronger hydrophobic interactions with the ligands of the AuTTMA scaffold. Therefore, it was concluded that the transformation of substrates takes place only after the dissociation of the FeTPP assemblies within the AuTTMA scaffold.

Further studies were performed using **Fe-NZ_37** as 37 °C is the ideal temperature for most bacterial and cell culture studies. This would allow us to elucidate the thermoresponsive behavior in biological environments. Temperature-controlled activation of the nanozymes was verified by comparing the catalytic activity of **Fe-NZ_37** with that of free FeTPP assemblies. As shown in **Figure 2b**, **Fe-NZ_37** was activated at 37 °C while free FeTPP solution was activated at 25 °C. Panels correspond to 60-minute exposure periods for each temperature. We also investigated the reversibility of thermoresponsive behavior using **Fe-NZ_37**. **Figure 2c** demonstrates the reversible nature of thermal activation of **Fe-NZ_37**, wherein the nanozyme can be returned to its dormant state by simply cooling the system.
We therefore conclude that confining FeTPP assemblies in the monolayer of our NPs produces nanozymes that respond to subtle changes in temperature by reversibly gating the access of substrates to active centers.

Elucidation of the thermal gating mechanism of thermoresponsive nanozymes

We studied the UV-Vis spectra of the nanozyme at different temperatures to validate that the mechanism of **Fe-NZ_37** activation is based on the dynamics of the confined FeTPP assemblies. Iron porphyrin aggregates present a characteristic absorption band (Soret band) located ~410 nm, that tends to increase in intensity and blue shift when such assemblies dissociate into smaller structures.[37] The spectra of **Fe-NZ_37** show the electronic transitions of both chromophores, the gold core, and the confined FeTPP assemblies (**SI-4**). The absorption bands of the NP scaffolds show minimal changes within the studied range of temperatures (**SI-3**), which allows their subtraction from the **Fe-NZ_37** spectra to provide more insight into the behavior of the confined FeTPP assemblies at different temperatures. The subtracted spectra of **Fe-NZ_37** is presented in (**Figure 3b**). At higher temperatures, the increased intensity of the Soret band is accompanied by a small blue shift. This behavior indicates that confined FeTPP assemblies dissociate at the increased temperatures. Analysis of the variations of intensity of the Soret band (412 nm) with temperature shows pronounced changes only when the temperature reaches the 37 °C turn-on temperature, consistent with porphyrin catalyst dissociation at the activation temperature (**Figure 3d**). Next, we analyzed variations in the Soret band of confined FeTPP assemblies in **Fe-NZ_37** when exposed to different cycles of heating (37 °C) and cooling (at 25 °C) (See **SI-4**). **Figure 3c** shows that the intensity of the Soret band reversibly increases at 37 °C and decreases at room temperature. These results are consistent with the observed reversible thermoresponsive behavior of the catalytic properties of **Fe-NZ_37** (**Figure 2d**). Resorufin showed no change in fluorescence due to changes in temperature (**SI-6**).

We next conducted ICP-MS experiments to detect whether the dissociation processes of the confined FeTPP assemblies occurred solely within the monolayer of the **Fe-NZ_37**, or if the catalysts could escape to solution. For this, **Fe-NZ_37** samples were incubated at 37 °C for 4 and 24h, then immediately filtered (Amicon® ultra 4, 10K). Samples remaining in the filters were then collected, digested and

analyzed by ICP. **Figure 3d** shows that the heated **Fe-NZ_37** samples display the same Fe:Au ratio (mol:mol) as the samples kept at RT. These results confirm that all dynamic processes detected by UV-Vis only occur within the confining environment of the monolayer of **Fe-NZ_37** as represented in **Figures 1d**. Furthermore, we demonstrated that only dissociated FeTPP contribute to catalysis. This can be seen in **SI-10** where upon heating all **Fe-NZs** to 45 °C, rate of catalysis is directly proportional to the amount of catalyst encapsulated in each of the **Fe-NZs.**

Thermoresponsive behavior of Fe-NZ_37 in biological systems

Having characterized our thermoresponsive nanozymes in solution, we subsequently studied potential for the eradication of bacterial biofilms. The temperature-dependent properties of **Fe-NZ_37** in the biofilm were evaluated through the catalytic deprotection of pro-Res as determined through confocal microscopy. Biofilms comprised of green fluorescent protein-expressing *E. coli* (GFP-*E. coli*) were incubated with **Fe-NZ_37** in M9 media for 1 h to allow internalization of nanozymes within the biofilms.[22] Bacterial biofilms were then washed three times with PBS to remove excess nanozyme. The thermoresponsive behavior of the internalized nanozymes was then tested by incubating the biofilms in M9 media containing pro-Res (10 μM) at 25 and 37 °C for ~ 1hr before obtaining the images shown in **Figure 4**. Biofilms incubated only with pro-Res served as the negative control.

Figure 4 shows confocal studies that examine the penetration of nanozymes into bacterial biofilms. By analyzing the green channel, the GFP-*E. coli* biofilms can be visualized (**Figure 4 b-i, c-i, and d-i**). Notably, the biofilms treated with **Fe-NZ_37** at 37 °C (**Figure 4 d-i**) resulted in higher bacterial density, presumably due to a combination of growth-stimulating effects (hormesis) of the cationic nanoparticles at low concentrations[24]. Analysis of the red channel illustrates negligible fluorescence in biofilms treated with pro-Res and **Fe-NZ_37** at 25 °C (**Figure 4 c-i**), and also those treated with only pro-Res at 37 °C (**Figure 4 b-i**). These results indicate that pro-Res deprotection occurs only in the presence of **Fe-NZ_37** at 37 °C. The merged channel shows that the generated red fluorophore co-localizes with GFP-*E. coli*, implying that it is being activated within the biofilm. This suggests that the nanozymes successfully penetrated the bacterial biofilms and were able to retain thermoresponsive catalytic activity within the biofilms.

From an antimicrobial perspective, a strategy that relies on pro-antibiotic activation through bioorthogonal thermoresponsive nanozymes can provide spatiotemporally controlled generation of antibiotics. As a result, these systems could facilitate the development of antimicrobial therapies with reduced side effects for mammalian tissues, organs, and beneficial microorganisms. We demonstrated this using **Fe-NZ_37** for the activation of pro-Mox (a protected moxifloxacin derivative) (**Figure 5** and **SI-8**).

E. coli biofilms, treated with **Fe-NZ_37** and different concentrations of pro-Mox, were incubated at 25 and 37 °C for 6 h. Following this, samples were washed with PBS, and their viability was analyzed through an alamarBlue assay. Biofilms treated with varying concentrations of pro-Mox only and **Fe-NZ_37** only were tested as negative controls and varying concentrations of Mox + **Fe-NZ_37** was used as a positive control.
Figure 5b and **5c** show the results obtained from bacterial biofilms exposed to each treatment described above at 25 and 37 °C respectively. As expected, samples treated with different concentrations of pro-Mox displayed negligible

variations in bacterial viability at both temperatures. On the contrary, biofilms responded in a dose-dependent manner to treatments containing **Fe-NZ_37** and different concentrations of active Mox, regardless of the temperature used. Biofilms treated with pro-Mox and **Fe-NZ_37** exhibited biofilm inhibitory effects at 37 °C in a dose dependent manner, while biofilms exposed to pro-Mox and **Fe-NZ_37** at 25 °C (Fig 5b, red bars) displayed no significant variations in viability. Notable bactericidal effect was registered with pro-Mox concentrations of above 2 μM. These results show that **Fe-NZ_37** can thermally regulate bioprocesses via the uncaging of modulatory drugs even in the presence of complex biological environments.

Conclusions

In this report, we highlight a strategy for fabricating thermoresponsive nanocatalysts that reversibly switch between dormancy and high rates of substrate processing, over slight variations in temperature. This strategy is based on the encapsulation of transition metal catalysts, in the form of supramolecular assemblies, into the monolayer of gold nanoparticles. We demonstrated that by confining supramolecular structures (p-p aggregates in our case) into semi-rigid biocompatible scaffolds the stimuli-responsive behavior of these supramolecular complexes is preserved in biological environments and can be employed in applications that include localized therapy and imaging. This enables the TMC assemblies to reversibly dissociate within the hosting scaffold upon heating, consequently resuming catalytic activity. This gating mechanism is based on the dynamics of confined TMC assemblies and allows the nanozymes to display thermoresponsive behavior in complex biological systems. Together with high rates of substrate processing, these properties make our nanozymes well-suited for biomedical applications that include not only antibacterial therapies, but also the self-modulation of inflammatory processes, which typically produce local heating. This strategy can be adapted to integrate other self-assembled chromophores and/or fluorescent molecules that can be used in the fabrication of nanometric sensors,[38, 39] that detect subtle changes in cellular microenvironments; and programable nanobots that exert preventive regulatory functions in biosystems. This work presents a blueprint for synthesizing a family of reversible thermoresponsive nanozymes with tailored activation temperatures and preserved biorthogonal activity in complex biological environments.

EXPERIMENTAL PROCEDURES

Synthesis and characterization of ligands, NPs (**Figure 1d**), nanozymes, and substrates are described in the Supplementary Information. Detailed sample preparation for ICP-MS, UV-Vis characterization of nanozymes and FeTPP assemblies, and additional bacteria culture studies can also be found in the Supplementary Information.

Fabrication of Thermoresponsive Nanozymes

0.5 mL of FeTPP solution in THF were mixed with an equal volume of aqueous solutions of NPs (10 μM) (See **SI-11,12** for AuTTMA synthesis), and stirred for 10 min. Following this, THF was slowly removed by evaporation to induce the encapsulation of FeTPP assemblies into the NP monolayer, with excess catalyst precipitating. **Fe-NZ** solutions were then purified by centrifugation at 14,000 rpm

to eliminate precipitated FeTPP and filtered (Amicon® ultra 4, 10K) six times to remove the remaining free catalyst. For synthesizing **Fe-NZ_37, Fe-NZ_34**, **Fe-NZ_31**, **Fe-NZ_28** and **Fe-NZ_25**, 1 mL of FeTPP solutions with concentrations of 2.84 mM, 284 μM, 28.4 μM, 2.84 μM and 0.28 μM respectively, were mixed with equal volume of NP solutions at 10 μM (**SI-12**). The resulting solutions were then concentrated by roto-evaporation and purified through multiple sessions of centrifugation and filtration (Amicon® ultra 4, 10K). For long term preservation of Fe-NZs solutions (1-2 month), solid ascorbic acid was added to stock solutions at concentrations ranging from 1-6 mg/mL.

Determination of temperature of activation of thermoresponsive nanozymes

Each kinetic experiment was performed in a 96-well black plate with 100 μL of PBS solution containing the corresponding **Fe-NZ** (50 nm), pro-Res (20 μM), and 5 mM of glutathione (See **SI-13** for pro-Res synthesis). Samples were then immediately inserted into the plate reader at 25 °C to analyze the evolution of fluorescence (Ex. 568 nm, Em. 588 nm). At the end of each 60-minute interval, the incubation temperature was increased by 3 °C, and fluorescence was analyzed for other 60 mins. When nanozymes were observed to become thermally active, fluorescence was monitored until reaching a maximum value (typically around 2000 a.u.) representing pro-Res total transformation.

Thermoresponsive activation of prodrug in bacterial biofilms

E. coli strains CD 2 and GFP-*E. coli* were inoculated in 3 mL LB broth and grown to the stationary phase at 37 °C. The cultures were then washed thrice in 0.85% sodium chloride solution through centrifugation. The concentration of the resuspended bacteria solutions was estimated by measuring the optical density at 600 nm. Seeding solutions for both strains were prepared by diluting to 0.1 OD_{600} (~10^8 colony forming units/ml) in M9 minimal media.

For the confocal studies, GFP-*E. coli* seeding solutions were spiked with IPTG (Isopropyl **β**-D-1-thiogalactopyranoside) so that the final solution contained 1mM of IPTG. 1 ml of the seeding solution was placed in confocal dishes and incubated at room temperature for ~3 days to grow biofilms. M9 minimal media was replaced each day. Biofilms were washed with PBS three times on day 3 and incubated with **Fe-NZ_37** in M9 media for 1 h. Bacterial biofilms were next washed three times with PBS to remove excess nanozyme and incubated pro-Res (100 μM) at 25 and 37 °C for ~1 hr before obtaining images.

For the biofilm viability studies, 100 μL of *E. Coli* (CD 2) seeding solutions was added into each well of a 96 well-plate and incubated overnight at room temperature to grow the biofilms. The biofilms were then washed thrice with PBS and treated with nanozymes (100 nM), and/or pro-Mox/Mox (See **SI-14** for pro-Mox synthesis) at varied concentrations prepared in M9 media. One set of plates was incubated at 37 °C for 5 h while the other was kept at 25 °C. After this treatment, the biofilms were washed with PBS three times and their viability was determined using the alamarBlue assay according to the protocol established by the manufacturer

SUPPLEMENTAL INFORMATION

Supplemental Information includes the following information - The synthesis and characterization of the materials used – nanoparticle, nanozyme, pro-Res, pro-Mox; UV-Vis characterization of the thermoresponsive behavior with appropriate controls

; Characterization of the therapeutic window between Mox and pro-Mox. Supplemental information can be obtained at - www.cell.com/chem/home.

ACKNOWLEDGMENTS

This work was supported by the NIH (EB022641) (GM008515, D.C.L.), Research Corporation for a TREE award (V.M.R.) and CHE-1808199 (V.M.R. and R.W.V.).

Correspondence and requests for materials should be addressed to V.M.R. (e-mail: rotello@chem.umass.edu).

AUTHOR CONTRIBUTIONS

R.C.-M., and V.M.R. conceived the idea. R.C.-M, L.D.H. R.H., R.F.L and X.Z. synthesized nanozymes and substrates. R.C.-M., L.D.H., and L.S.W. designed and performed the experiments in solutions. R.C.-M., S. G., R.H., J.M.M., and C.H.L. conceived and designed bacteria experiments. R.C.-M., L.C., D.C.L., R.W.V., conceived and performed ICP-MS analyses. All authors analyzed and discussed the data. R.C.-M., L.D.H, S. G., and V.M.R. co-wrote the manuscript.

DECLARATION OF INTERESTS

The authors declare no competing interests.

REFERENCES AND NOTES

1. Unciti-Broceta, A., Johansson, E.M. V, Yusop, R.M., Sánchez-Martín, R.M., and Bradley, M. (2012). Synthesis of polystyrene microspheres and functionalization with Pd0 nanoparticles to perform bioorthogonal organometallic chemistry in living cells. Nat. Protoc. *7*, 1207–1218.

2. Weiss, J.T., Dawson, J.C., Macleod, K.G., Rybski, W., Fraser, C., Torres-Sánchez, C., Patton, E.E., Bradley, M., Carragher, N.O., and Unciti-Broceta, A. (2014). Extracellular palladium-catalysed dealkylation of 5-fluoro-1-propargyl-uracil as a bioorthogonally activated prodrug approach. Nat. Commun. *5*, 3277.

3. Yusop, R.M., Unciti-Broceta, A., Johansson, E.M. V., Sánchez-Martín, R.M., and Bradley, M. (2011). Palladium-mediated intracellular chemistry. Nat. Chem. *3*, 239–243.

4. Völker, T., and Meggers, E. (2015). Transition-metal-mediated uncaging in living human cells—an emerging alternative to photolabile protecting groups. Curr. Opin. Chem. Biol. *25*, 48–54.

5. Bai, Y., Chen, J., and Zimmerman, S.C. (2018). Designed transition metal catalysts for intracellular organic synthesis. Chem. Soc. Rev. *47*, 1811–1821.

6. Zhang, X., Huang, R., Gopalakrishnan, S., Cao-Milán, R., and Rotello, V.M. (2019). Bioorthogonal Nanozymes: Progress towards Therapeutic Applications. Trends Chem. *1*, 90–98.

7. Cao-Milán, R., He, L.D., Shorkey, S., Tonga, G.Y., Wang, L.-S., Zhang, X., Uddin, I., Das, R., Sulak, M., and Rotello, V.M. (2017). Modulating the catalytic activity of enzyme-like nanoparticles through their surface functionalization. Mol. Syst. Des. Eng. *2*, 624–628.

8. Brändel, T., Sabadasch, V., Hannappel, Y., and Hellweg, T. (2019). Improved Smart Microgel Carriers for Catalytic Silver Nanoparticles. ACS Omega *4*, 4636–4649.

9. Yu Mei, Yan Lu, Frank Polzer, and, Ballauff*, M., and Drechsler, M. (2007). Catalytic Activity of Palladium Nanoparticles Encapsulated in Spherical Polyelectrolyte Brushes and Core−Shell Microgels.

10. Jia, H., Cao, J., and Lu, Y. (2017). Design and fabrication of functional hybrid materials for catalytic applications. Curr. Opin. Green Sustain. Chem. *4*, 16–22.

11. Lu, Y., Proch, S., Schrinner, M., Drechsler, M., Kempe, R., and Ballauff, M. (2009). Thermosensitive core-shell microgel as a "nanoreactor" for catalytic active metal nanoparticles. J. Mater. Chem. *19*, 3955.

12. Drechsler, U., Erdogan, B., and Rotello, V.M. (2004). Nanoparticles: Scaffolds for Molecular Recognition. Chem. - A Eur. J. *10*, 5570–5579.

13. Canaparo, R., Foglietta, F., Giuntini, F., Pepa, C. Della, Dosio, F., and Serpe, L. (2019). Recent developments in antibacterial therapy: Focus on stimuli-responsive drug-delivery systems and therapeutic nanoparticles. Molecules 24.

14. Dos Santos Ramos, M.A., Da Silva, P.B., Spósito, L., De Toledo, L.G., Bonifácio, B. vidal, Rodero, C.F., Dos Santos, K.C., Chorilli, M., and Bauab, T.M. (2018). Nanotechnology-based drug delivery systems for control of microbial biofilms: A review. Int. J. Nanomedicine 13, 1179–1213.

15. Canaparo, R., Foglietta, F., Giuntini, F., Pepa, C. Della, Dosio, F., and Serpe, L. (2019). Recent developments in antibacterial therapy: Focus on stimuli-responsive drug-delivery systems and therapeutic nanoparticles. Molecules 24.

16. Jia, H., Roa, R., Angioletti-Uberti, S., Henzler, K., Ott, A., Lin, X., Möser, J., Kochovski, Z., Schnegg, A., Dzubiella, J., *et al.* (2016). Thermosensitive Cu2O–PNIPAM core–shell nanoreactors with tunable photocatalytic activity. J. Mater. Chem. A *4*, 9677–9684.

17. Liu, G., Wang, D., Zhou, F., and Liu, W. (2015). Electrostatic Self-Assembly of Au Nanoparticles onto Thermosensitive Magnetic Core-Shell Microgels

for Thermally Tunable and Magnetically Recyclable Catalysis. Small *11*, 2807–2816.

18. Hamamoto, H., Suzuki, Y., Yamada, Y.M.A., Tabata, H., Takahashi, H., and Ikegami, S. (2005). A Recyclable Catalytic System Based on a Temperature-Responsive Catalyst. Angew. Chemie Int. Ed. *44*, 4536–4538.

19. Hong, M.C., Choi, M.C., Chang, Y.W., Lee, Y., Kim, J., and Rhee, H. (2012). Palladium Nanoparticles on Thermoresponsive Hydrogels and their Application as Recyclable Suzuki-Miyaura Coupling Reaction Catalysts in Water. Adv. Synth. Catal. *354*, 1257–1263.

20. Zhang, J., Zhang, M., Tang, K., Verpoort, F., and Sun, T. (2014). Polymer-Based Stimuli-Responsive Recyclable Catalytic Systems for Organic Synthesis. Small *10*, 32–46.

21. Shabbir, S., Lee, Y., and Rhee, H. (2015). Au(III) catalyst supported on a thermoresponsive hydrogel and its application to the A-3 coupling reaction in water. J. Catal. *322*, 104–108.

22. van Rhee, P.G., Rikken, R.S.M., Abdelmohsen, L.K.E.A., Maan, J.C., Nolte, R.J.M., van Hest, J.C.M., Christianen, P.C.M., and Wilson, D.A. (2014). Polymersome magneto-valves for reversible capture and release of nanoparticles. Nat. Commun. *5*, 5010.

23. Díaz Díaz, D., Kühbeck, D., and Koopmans, R.J. (2011). Stimuli-responsive gels as reaction vessels and reusable catalysts. Chem. Soc. Rev. *40*, 427–448.

24. Wang, L., Chen, S., Zhou, J., Yang, J., Chen, X., Ji, Y., Liu, X., Zha, L., Wang, L., Chen, S., *et al.* (2017). Silver Nanoparticles Loaded Thermoresponsive Hybrid Nanofibrous Hydrogel as a Recyclable Dip-Catalyst with Temperature-Tunable Catalytic Activity.

25. Elsevier Science (Firm), Y.-Y., Liu, X.-Y., Yang, J.-M., Lin, D.-L., Chen, X., and Zha, L.-S. (2012). Colloids and surfaces. A, Physicochemical and engineering aspects. (Elsevier Science Pub. Co)

26. Hamamoto, H., Suzuki, Y., Takahashi, H., and Ikegami, S. (2007). A New Solid-Phase Reaction System Utilizing a Temperature- Responsive Catalyst: Oxidative Cyclization with Hydrogen Peroxide. Adv. Synth. Catal. *349*, 2685–2689.

27. Tang, Y., Wu, T., Hu, B., Yang, Q., Liu, L., Yu, B., Ding, Y., and Ye, S. (2015). Synthesis of thermo- and pH-responsive Ag nanoparticle-embedded hybrid microgels and their catalytic activity in methylene blue reduction. Mater. Chem. Phys. *149–150*, 460–466.

28. De, M., Ghosh, P.S., and Rotello, V.M. (2008). Applications of Nanoparticles in Biology. Adv. Mater. *20*, 4225–4241.

29. Deng, Y.H., Yang, W.L., Wang, C.C., and Fu, S.K. (2003). A Novel Approach for Preparation of Thermoresponsive Polymer Magnetic Microspheres with Core–Shell Structure. Adv. Mater. *15*, 1729–1732.

30. Tonga, G.Y., Jeong, Y., Duncan, B., Mizuhara, T., Mout, R., Das, R., Kim, S.T., Yeh, Y.-C., Yan, B., Hou, S., *et al.* (2015). Supramolecular regulation of bioorthogonal catalysis in cells using nanoparticle-embedded transition metal catalysts. Nat. Chem. *7*, 597–603.

31. Jeong, Y., Tonga, G.Y., Duncan, B., Yan, B., Das, R., Sahub, C., and Rotello, V.M. (2018). Solubilization of Hydrophobic Catalysts Using Nanoparticle Hosts. Small *14*, 1702198.

32. Gupta, A., Das, R., Yesilbag Tonga, G., Mizuhara, T., and Rotello, V.M. (2018). Charge-Switchable Nanozymes for Bioorthogonal Imaging of Biofilm-Associated Infections. ACS Nano *12*, 89–94.

33. Jackson, A.M., Myerson, J.W., and Stellacci, F. (2004). Spontaneous assembly of subnanometre-ordered domains in the ligand shell of monolayer-protected nanoparticles. Nat. Mater. *3*, 330–336.

34. Fidalgo-Marijuan, A., Barandika, G., Bazán, B., Urtiaga, M.K., Lezama, L., and Arriortua, M.I. (2013). Fe–TPP Coordination Network with Metalloporphyrinic Neutral Radicals and *Face-to-Face* and *Edge-to-Face* π–π Stacking. Inorg. Chem. *52*, 8074–8081.

35. Nozawa, R., Tanaka, H., Cha, W.-Y., Hong, Y., Hisaki, I., Shimizu, S., Shin, J.-Y., Kowalczyk, T., Irle, S., Kim, D., *et al.* (2016). Stacked antiaromatic porphyrins. Nat. Commun. *7*, 13620.

36. Sasmal, P.K., Carregal-Romero, S., Han, A.A., Streu, C.N., Lin, Z., Namikawa, K., Elliott, S.L., Köster, R.W., Parak, W.J., and Meggers, E. (2012). Catalytic Azide Reduction in Biological Environments. ChemBioChem *13*, 1116–1120.

37. Satake, A., and Kobuke, Y. (2007). Artificial photosynthetic systems: assemblies of slipped cofacial porphyrins and phthalocyanines showing strong electronic coupling. Org. Biomol. Chem. *5*, 1679.

38. Cao, C., and Long, Y.T. (2018). Biological Nanopores: Confined Spaces for Electrochemical Single-Molecule Analysis. Acc. Chem. Res. 51, 331–341.

39. Fu, K., Han, D., Ma, C., and Bohn, P.W. (2016). Electrochemistry at single molecule occupancy in nanopore-confined recessed ring-disk electrode arrays. Faraday Discuss. 193, 51–64.

FIGURE AND SCHEME TITLES AND LEGENDS

Figure 1| Thermoresponsive nanozyme design. a a) Structure of FeTPP. b) Conversion of profluorophore pro-Res through the catalytic reduction of aryl azides. c) Structure of AuTTMA d) Confined dynamics of FeTPP assemblies within AuTTMA monolayer; FeTPP forms a packed structure with ligands preventing substrates from reaching active sites. Increasing temperature triggers the dissociation of FeTPP assemblies and redistribution of FeTPP molecules within the monolayer, forming structures that allow substrates to access active centers, enabling catalysis. This process is reversed by cooling down the system.

Figure 2| Demonstrating the tunability and reversibility of the catalytic activity of thermoresponsive nanozymes. a) The thermoresponsive behavior of **Fe-NZ_25**, **Fe-NZ_28**, **Fe-NZ_31**, **Fe-NZ_34** and **Fe-NZ_37** was monitored by measuring the catalytic activity of each nanozyme (at equal concentrations) in the temperature range of 25-37 °C. Nanozymes were exposed to 25, 28, 31, 34 and 37 °C for a fixed time interval (60 min each except at 25 °C), represented by the appropriately colored panels. **b)** Thermal activation of the catalytic properties of **Fe-NZ_37** (red) at 37 °C compared with free FeTPP (blue). Each panel represents a 60 min period (except for the red panel) of exposure to a given temperature. **Fe-NZ_37** is only active at 37 °C (red panel) while free FeTPP (blue plot) displays catalytic activity even at 25 °C. **c)** Reversibility of catalytic properties of **Fe-NZ_37** was monitored through changes in catalytic activity due to alternate heating (to 37 °C) and cooling (to 25 °C) of Fe-NZ_37. Increase in fluorescence intensity is observed upon heating. Exposure to both temperatures was limited to a duration of 20 min each as denoted by the alternately colored panels. Experiments were conducted in PBS (pH = 7.4 solutions containing glutathione 5 mM as a cofactor for the catalytic process. Each experiment was replicated thrice, and error bars represent standard deviations of these measurements.

Figure 3| Thermally triggered reversible dissociation of FeTPP assemblies in the monolayer of NPs a) Scheme of **Fe-NZ_37** at temperatures below (blue panel) and above (above) 37 °C. **b)** Subtracted UV-Vis spectra of **Fe-NZ_37** at different temperatures. Inset, intensity of 412 nm band with increment of temperature. Significant variations in A_{412} are observed for **Fe-NZ_37** at temperatures above 37 °C (red panel). **c)** Intensity of the band at 412 nm during cycles of heating at 37 °C (red circles) and cooling at 25 °C (blue circles). Iron/Au ratio of **Fe_NZ-37** solutions subjected to 37 °C (for different lapse of time) and to 25 °C. Measurements were conducted by ICP-MS. Each experiment was made in triplicate. Error bars represent standard deviations of these measurements.

Figure 4| Thermoresponsive behavior of nanozymes in biofilms. a) Internalization of **Fe-NZ_37** in biofilms and temperature-controlled activation of pro-Res. Confocal microscopy images of biofilms (b) treated with pro-Res at 37 °C, (c) with a combination of **Fe-NZ_37**, and (d) pro-Res at 25 °C, and with a combination of **Fe-NZ_37** and pro-Res at 37 °C. Each channel is represented with sub index -i (green), -ii (red), and -iii (merged). Bars represent 50 μM.

Figure 5| Deprotection of antimicrobials in biofilms using thermoresponsive nanozymes. Fe-NZ_37 was used for the controlled activation of antimicrobial prodrugs that modulate biofilms viability. a) Scheme of activation of pro-Mox by **Fe-NZ_37** at 37 °C. b) *E. coli* biofilms treated with pro-Mox and **Fe-NZ_37** (red bars) at 25 °C, and c) at 37 °C. Biofilms treated only with pro-Mox (blue bars) or with a combination of Mox and **Fe-NZ_37** (pink bars) were used in all experiments as negative and positive controls, respectively. Each experiment was replicated five times. Error bars represent standard deviations of these measurements. The thermoresponsive properties of **Fe-NZ_37** combined with its ability to penetrate biofilms is ideal for controlled deprotection of pro-Mox within biofilms. Moxifloxacin (Mox) was chosen as the antibacterial agent (**Figure 5a**, right) due to its broad-spectrum activity.[39] The secondary amino group is crucial for binding two target enzymes of the drug[25]. Masking this group with the bulky aryl-azide carbamate (**Figure 5a**, left) reduces the antibiotic activity of this drug by more than two orders of magnitude, as can be seen in **SI-7**. This large reduction in the bactericidal activity of pro-Mox (with respect to Mox) makes it ideal in combination with **Fe-NZ_37** to thermally control the viability of bacterial biofilms.

Figure 1

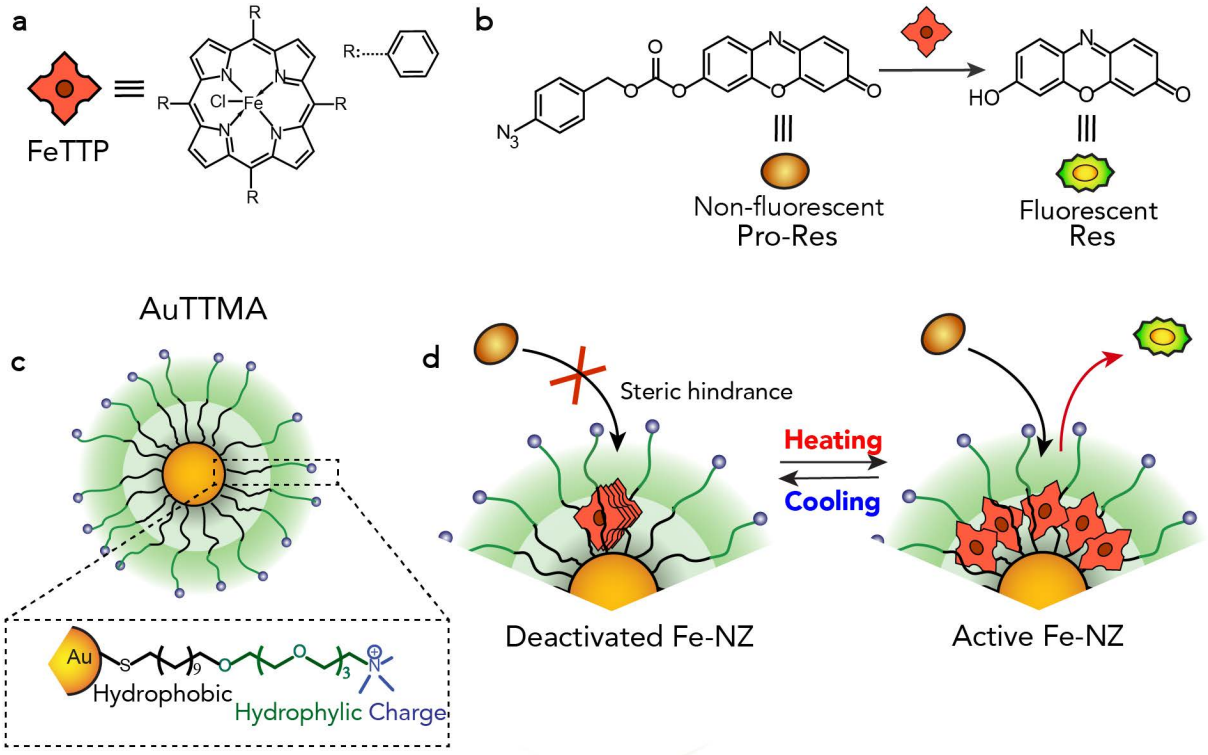

Figure 2

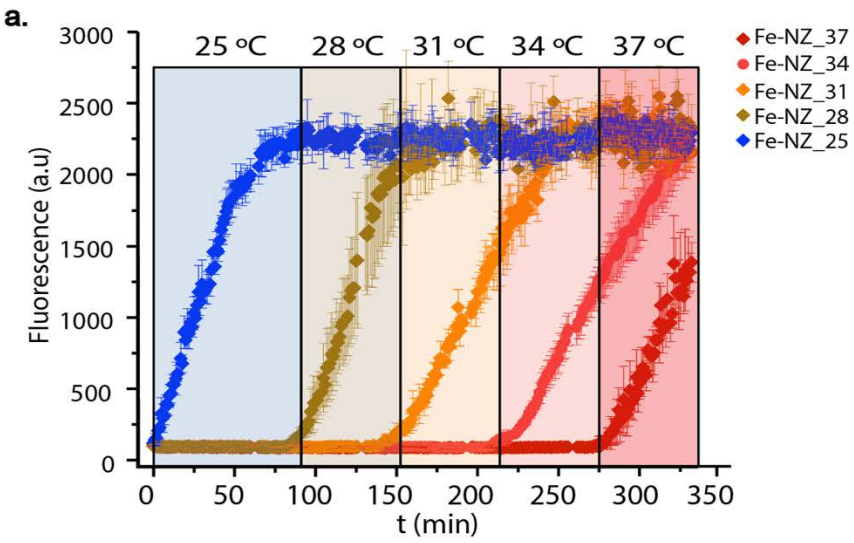
a.
25 °C
28 °C
31 °C
34 °C
37 °C
Fe-NZ_37
Fe-NZ_34
Fe-NZ_31
Fe-NZ_28
Fe-NZ_25
Fluorescence (a.u)
t (min)

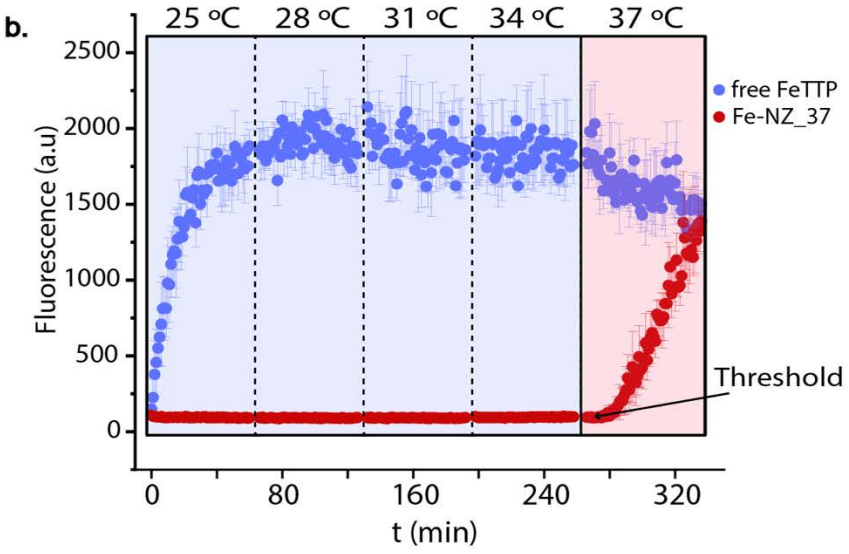
b.
25 °C
28 °C
31 °C
34 °C
37 °C
free FeTTP
Fe-NZ_37
Threshold
Fluorescence (a.u)
t (min)

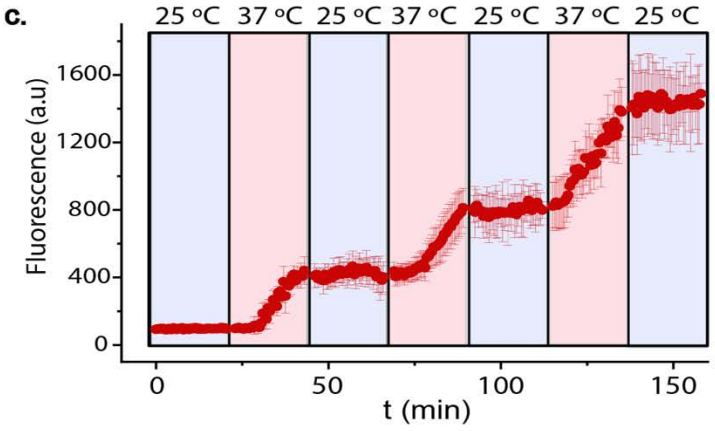
c.
25 °C
37 °C
25 °C
37 °C
25 °C
37 °C
25 °C
Fluorescence (a.u)
t (min)

Figure 3

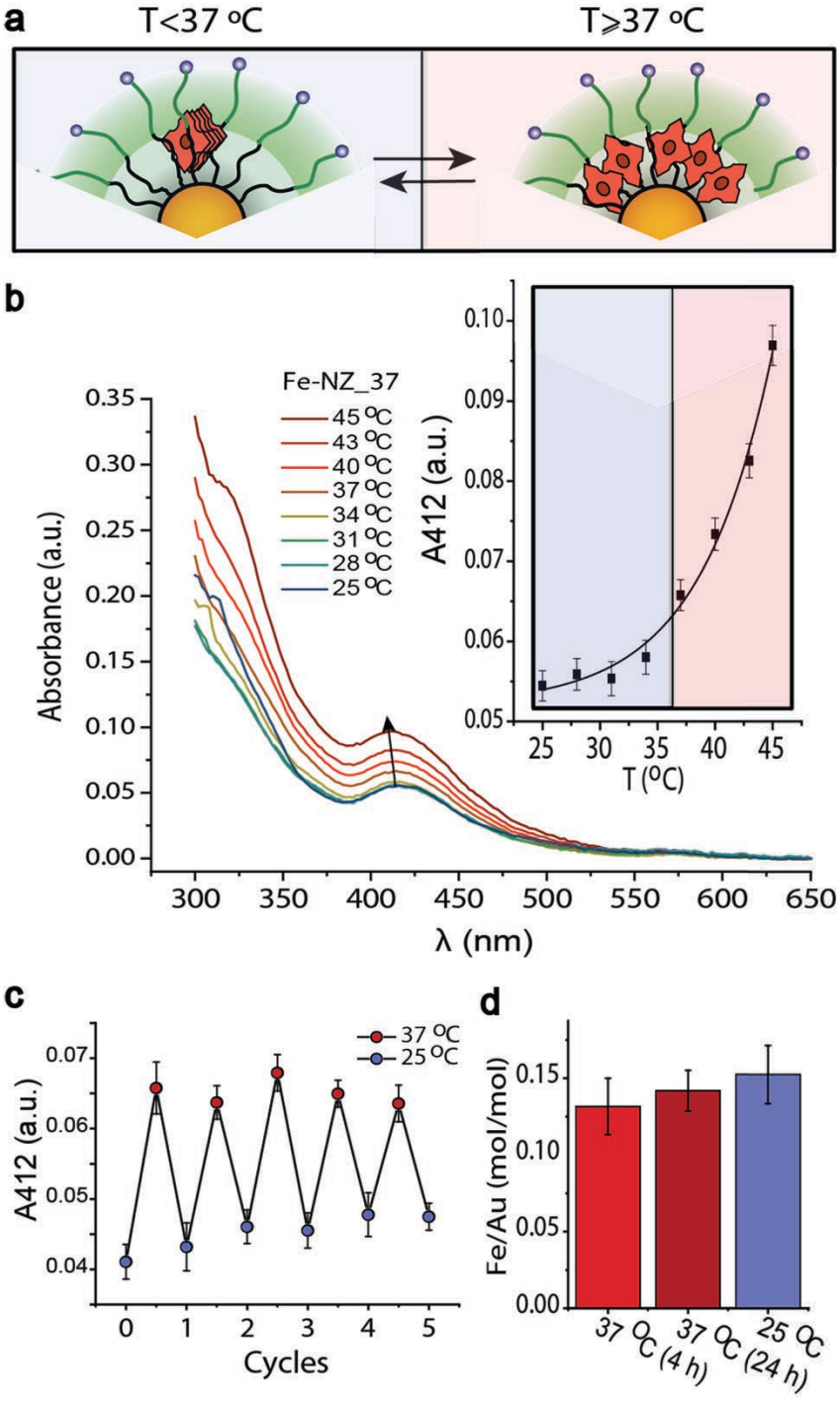
a
T<37 ºC
T⩾37 ºC
b
Fe-NZ_37
45 ºC
43 ºC
40 ºC
37 ºC
34 ºC
31 ºC
28 ºC
25 ºC
Absorbance (a.u.)
λ (nm)
A412 (a.u.)
T (ºC)
c
37 ºC
25 ºC
A412 (a.u.)
Cycles
d
Fe/Au (mol/mol)
37 ºC (4 h)
37 ºC (24 h)
25 ºC

Figure 4

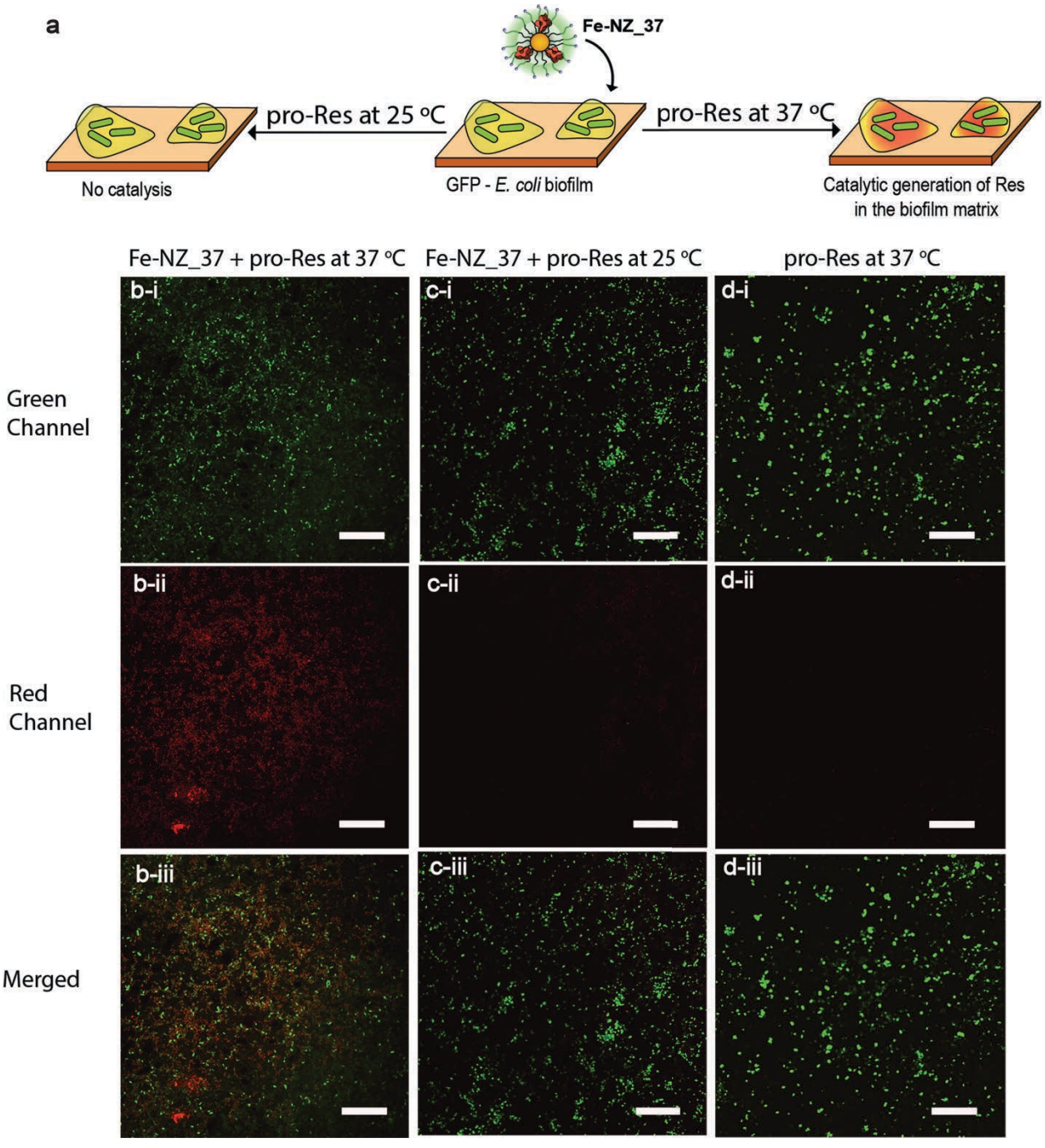
a
Fe-NZ_37
pro-Res at 25 °C
pro-Res at 37 °C
No catalysis
GFP - E. coli biofilm
Catalytic generation of Res in the biofilm matrix
Fe-NZ_37 + pro-Res at 37 °C
Fe-NZ_37 + pro-Res at 25 °C
pro-Res at 37 °C
Green Channel
Red Channel
Merged
b-i
c-i
d-i
b-ii
c-ii
d-ii
b-iii
c-iii
d-iii

Figure 5

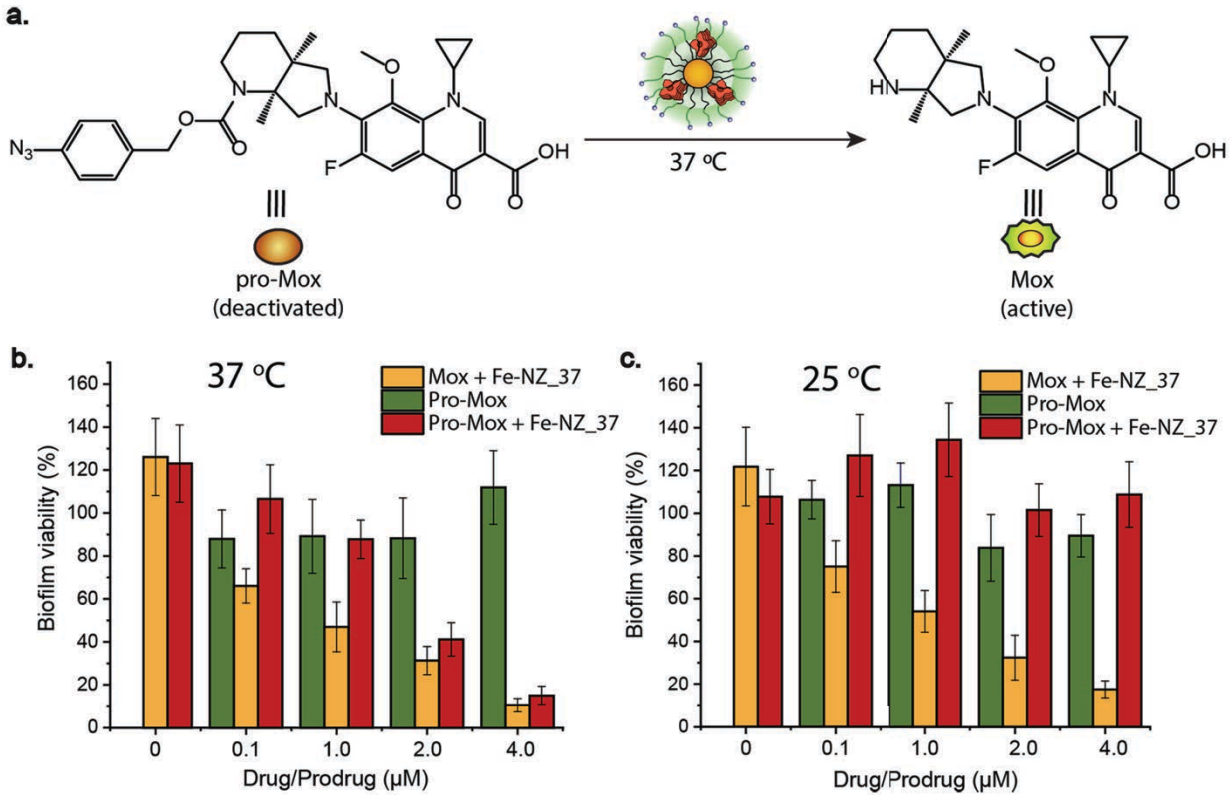
a.
pro-Mox
(deactivated)
37 °C
Mox
(active)
b.
37 °C
Mox + Fe-NZ_37
Pro-Mox
Pro-Mox + Fe-NZ_37
Biofilm viability (%)
Drug/Prodrug (μM)
c.
25 °C
Mox + Fe-NZ_37
Pro-Mox
Pro-Mox + Fe-NZ_37
Biofilm viability (%)
Drug/Prodrug (μM)